

## **Views from EPOXI: Colors in our Solar System as an Analog for Extrasolar Planets**

Carolyn A. Crow<sup>1</sup>, L. A. McFadden<sup>2</sup>, T. Robinson<sup>3</sup>, T. A. Livengood<sup>4</sup>, T. Hewagama<sup>1</sup>, R. K. Barry<sup>2</sup>, L. D. Deming<sup>2</sup>, V. Meadows<sup>3</sup>, C. M. Lisse<sup>5</sup>

<sup>1</sup>University of Maryland, <sup>2</sup>Goddard Space Flight Center, <sup>3</sup>University of Washington, <sup>4</sup>NCESSE, <sup>5</sup>APL

Carolyn A. Crow  
*Faculty Research Assistant*  
*University of Maryland, College Park, MD 20740, USA*

Lucy-Ann McFadden  
*Chief of University and Post-doctoral Programs*  
*NASA Goddard Space Flight Center, Greenbelt, MD 20771, USA*

Tyler D. Robinson  
*Graduate Researcher*  
*University of Washington, Seattle, WA 98195-1580, USA*

Timothy A. Livengood  
*Senior Research Scientist*  
*National Center for Earth and Space Science Education and*  
*NASA Goddard Space Flight Center, Greenbelt, MD 20771 USA*

Tilak Hewagama  
*Research Scientist*  
*University of Maryland, College Park, MD 20740, USA*

Richard K. Barry  
*Research Astrophysicist*  
*NASA Goddard Space Flight Center, Greenbelt, MD 20771, USA*

L. Drake Deming  
*Senior Scientist for Exo-Planet Research*  
*NASA Goddard Space Flight Center, Greenbelt, MD 20771, USA*

Victoria Meadows  
*Associate Professor*  
*University of Washington, Seattle, WA 98195-1580, USA*

Carey M. Lisse  
*Senior Research Scientist*  
*Johns Hopkins University/Applied Physics Lab, Laurel, MD 20723, USA*

## **I. Introduction**

With extrasolar planet detection becoming more commonplace, the frontiers of extrasolar planet science have moved beyond detection to the observations required to determine planetary properties. Once the existing observational challenges have been overcome, the first visible-light studies of extrasolar Earth-sized planets will likely employ filter photometry or low-resolution spectroscopy to observe disk-integrated radiation from the unresolved planet. While spectroscopy of these targets is highly desirable (e.g. Des Marais 2002), and provides the most robust form of characterization, S/N considerations presently limit spectroscopic measurements of extrasolar worlds. Broadband filter photometry will thus serve as a first line of characterization.

The most ambitious mission concepts for visible light spectroscopic and photometric characterization of extrasolar planets include large space based telescopes that will employ coronagraphic imagers or occulter (e.g. Levine et al., 2009; Cash, 2006) to greatly reduce the brightness of the parent star and reveal the fainter planet (Trauger & Traub, 2007). The James Webb Space Telescope, currently under construction and planned to launch in 2014, may provide a more immediate coronagraphic capability for extrasolar planet studies if it can be paired with a free flying occulter spacecraft (Soummer et al., 2009).

Visual inspection of Solar System planets reveals an array of planetary colors, resulting from the diversity of atmospheric and surface composition and structure. While this handful of planets will not fully represent the diversity to be found even in the 430+ planets now known, these are the only ones for which we can currently obtain multi-wavelength visible photometry.

Previous attempts to obtain disk-integrated spectra or photometry of the Earth and Mars have been made by interplanetary spacecraft en route to other targets in the Solar System. The first spacecraft mission dedicated to whole-disk Earth observations as a principal scientific goal is the Extrasolar Observation and Characterization (EPOCH) investigation, which is part of NASA's EPOXI mission (Ballard, 2009; Cowan, 2009). EPOCH utilized the Deep Impact (DI) flyby spacecraft to provide time-resolved multi-wavelength medium-band filter photometry and moderate-resolution spectroscopy of the Earth as an analog experiment for photometric observations of an extrasolar Earth-like planet. These data were taken from distances of 0.18-0.3 AU, providing multi-wavelength coverage of five full rotations of the Earth from equatorial and polar views, and over several seasons (Livengood et al., 2010). EPOCH observed a transit of the Earth by the Moon in May 2008, facilitating a comparison between two terrestrial bodies with significantly differing surface properties (Deming et al. 2007). Near the end of the mission, medium-band filter photometry of Mars was also obtained.

In this paper we use EPOCH filter photometry of the Earth, Moon and Mars, model spectra, and previous photometric and spectroscopic observations of a range the solar system planets, Titan, and Moon to explore the limitations of using color as a baseline for

The EPOCH investigation planned five observations of Earth for 2008. EarthObs4, presented here, was conducted over exactly 24 hours beginning approximately 20:00 UT, 28 May 2008 and included a transit of Earth by the Moon, see Figure 1a. This sequence provided contemporaneous photometry and spectroscopy of the Moon and Earth. It also allowed for observations of the far side of the Moon, which is not visible from Earth due to the Moon's synchronous rotation. The illuminated region of the Moon in the May 2008 images spanned from 160° W to 260° W longitudes (approximately half of the lunar far side) and the phase angle for both Earth and Moon averaged 75.1°. An additional set of calibration data from January 16, 2005 was used to analyze the near side lunar reflectance for comparison with the far side data. Approximately 2/3 of the illuminated surface of the front side of the Moon was visible in the calibration images and encompassed the southeast near side Balmer crater regions, see Figure 1b (Maxwell & Andre 1981). The phase angle for these images was 97.6°. In addition to lunar and Earth data, we analyzed 64 sets of full-disk observations of Mars collected over a 24-hour period starting on November 20, 2009. The observations covered a nearly complete rotation period of Mars at a phase angle of 37° (Figure 1c). See Table 1 for details on observation parameters for all data sets.

**Figure 1a,b,c**

**Table 1**

The EPOCH observations were taken using the High Resolution Instrument (HRI) on the Deep Impact flyby spacecraft (Hampton et al. 2005), a 0.3m f/35 optical Cassegrain telescope equipped with a 9-position filter wheel and CCD camera. Two of the positions have broadband white light filters centered at 650 nm and the other seven are medium-band filters with 100nm bandwidths evenly spaced between 300 – 1000 nm (Hampton et al. 2005). Images of the Earth and Moon were taken through the 350, 750 and 950 nm filters hourly and through the remaining medium-band filters every 15 minutes, with exposure times ranging from 8-73 ms depending on the filter throughputs. See Table 2 for a list of filter center wavelengths and exposure times. We used eight of the 12 sets of lunar transit observations for our analysis. The remaining four sets were discarded because either the Moon was transiting Earth or the gradient of scattered Earthlight across the Moon was too large for a single background value subtraction.

**Table 2**

### **3. EPOXI Data Processing**

The raw data from the DI spacecraft are processed through a calibration pipeline that converts the raw data numbers into measured flux in units of W/m<sup>2</sup>/sr for a given bandpass. In the pipeline, the images are first decompressed, saturated pixels are flagged, and a dark frame is subtracted. Crosstalk functions are then applied to eliminate ghosts of the other three quadrants of the CCD, and the images are divided by the flat field to mitigate pixel-to-pixel variations. The HRI uses a frame-transfer CCD, so a desmearing process is necessary to correct for residual persistent smear left by bright objects during

surface composition and the texture of their regolith (Soderblom 1992; Roush et al. 1993; McKay et al. 1993). Each body experienced differentiation soon after it formed, followed by an extended period of regolith formation primarily from repeated impacts during the Late Heavy Bombardment period of solar system evolution (3.8-4.1 Gy ago) (Tera et al. 1974). Photons hitting the regolith surface are both scattered from grain boundaries and absorbed and reradiated after interacting with the minerals in the soil (Burns 1993; Hapke 2001).

In the case of the Moon, the regolith contains minerals, glass and nano-phase iron (Pieters et al. 2000). The steep slope towards the NIR in the lunar data is primarily due to the continuously varying absorption coefficient of nanophase iron that is produced by reduction of Fe and vapor deposition resulting from micrometeorite bombardment of the lunar surface. A large portion of the observed region of the lunar far side encompasses the South Pole Aitken Basin, which is enriched in mafic minerals relative to the near side (Nakamura et al. 2009). Charge transfer interactions with  $\text{Fe}^{2+}$  on the surface are responsible for the 950 nm absorption in the lunar spectrum (Lucey et al. 1998). It is important to note here that the 950 nm absorption cannot be due to the hydrated materials on the surface of the Moon detected by Sunshine et al. (2009) using the DI Medium Resolution Instrument (MRI) and the high-resolution near-IR spectrometer. The amount of lunar water is too small for its absorption effects to be measurable in the low spectral resolution HRI filter data.

In the case of Mars, the surface likely consists of fine-grained loess-like material as discussed in Singer et al. (1992). Surface mineral components containing optically active absorption bands in the visible are a combination of charge transfer absorption and spin-forbidden crystal field transitions due to  $\text{Fe}^{3+}$  and  $\text{Fe}^{2+}$  cations in ilmenite and pyroxene minerals. If the linear nature of the UV absorption in the lunar spectrum is indicative of the presence of nano-phase iron, it would appear that the disk-integrated Mars spectrum is not influenced by nano-phase iron.

#### **Figure 4**

##### *4.2. The Earth*

The disk-integrated reflectance spectrum of Earth shown in Figure 4 exhibits a steep incline towards UV wavelengths and is relatively flat at green to NIR wavelengths. The flat shape of the spectrum at longer wavelengths is attributed to clouds. Although, a slight rise in Earth's reflectivity from the 650 nm filter to the 850 nm filter is due to the fact that many surfaces on Earth (e.g., soils, sands, vegetation) are more reflective at NIR wavelengths than at visible wavelengths. An absorption feature can be seen in the 950 nm filter due to a strong water band located within this wavelength range (Traub 2003).

The increase in Earth's reflectance towards the UV is the result of Rayleigh scattering in the atmosphere. To investigate the significance of Rayleigh scattering in our Earth data, we produced two simulated high-resolution Earth spectra using the NASA Astrobiology Institute's Virtual Planetary Laboratory (VPL) 3-D spectral Earth model (Robinson et al. 2010) and convolved them with the HRI filter transmission curves, see Figure 5. In the first spectrum (solid line), realistic Rayleigh scattering is assumed and a rise in

comparison with the EPOCH data. Figure 6 shows a comparison between the EPOCH and Irvine data sets.

### Figure 6

The terrestrial worlds, other than the Earth, are all less reflective in the UV than in the NIR. Mercury, an airless body, has a reflectance spectrum increasing steadily from the UV to the IR due to light interactions with surface minerals (Vilas 1985). The Mercurian soil is low in Fe with  $> 2-3$  wt% at its surface, so Fe is not a major contributor to charge transfer slope in the reflectance of Mercury (McClintock et al. 2008). The visible colors of Mercury are not diagnostic of the surface mineral composition.

The reflectivity of Venus shows a depression in the UV and a relatively flat reflectance from the Green and NIR filters. Venus has a thicker atmosphere unlike the airless bodies discussed previously, so its atmospheric structure and composition are solely responsible for the planet's colors. Venus' opaque atmosphere contains several distinct layers of sulphuric acid clouds, which are distinguished by their aerosol particle size. The cloud deck which is primarily responsible for Venus' high reflectivity is located between about 50-80 km in altitude (Marov et al., 1973; Marov, 1978). Extinction optical depths through the Venusian haze (which extends up to about 90 km in altitude) and the upper cloud deck reach unity by about 30mbar (Knollenberg et al. 1980), so no appreciable amount of Rayleigh scattering can occur. The effects of a "UV absorber" can be seen in the reflectance spectrum of Venus bluewards of about 650 nm. The absorption efficiency of this substance increases between 650 to 300 nm, explaining the drop in Venus' reflectivity at blue wavelengths (Pollack et al. 1980). The flat reflectance of Venus' reflectivity curve beyond about 650 nm is explained by the sulphuric acid droplets' essentially non-absorptive behavior at visible wavelengths (Crisp 1986).

In addition to Irvine's photometric data, we used high spectral resolution, full-disk reflectance data for Jupiter, Saturn, Uranus, Neptune, and Titan from Karkoschka (1994). The observations were collected at the European Southern Observatory and span the wavelength range of 300 to 1000 nm at phase angles of  $9.8^\circ$ ,  $2.7^\circ$ ,  $0.6^\circ$ ,  $0.4^\circ$ , and  $2.7^\circ$ , respectively. We convolved these spectra with the HRI filter transmission curves to determine the medium band reflectance spectra of the five bodies. An overlay of the high-resolution reflectance spectrum of Jupiter from Karkoschka (1994) and the HRI filter transmission curves are seen in Figure 7 and the computed broadband photometric reflectance values for the Jovian worlds are shown in Figure 8.

### Figure 7

Uranus and Neptune are unique in that their reflectance spectra are relatively flat at blue and UV wavelengths while containing strong absorption features in the red and NIR. A perfectly scattering, semi-infinite atmosphere consisting of pure  $H_2$  would have a wavelength-independent, zero-phase reflectance of about 0.8 (Prather 1974), which is about 30-40% larger than the reflectance values reported by Karkoschka (1994, 1998) for Uranus and Neptune at short wavelengths. The discrepancy between the theoretical value

McKay 1995; Tomoasko et al. 2008). As a result, Titan's reflectance spectrum decreases steadily from 650 nm to UV wavelengths. Methane absorption dominates Titan's reflectance spectrum longward of 650 nm. Although these features are not as strong as those in the spectra of Uranus and Neptune, the 850nm and 950nm HRI filters show marked decreases in Titan's reflectance due to methane absorption.

## 5. Discussion

The objective of our study was to analyze the colors of the planets within our solar system and use them to create a baseline for characterizing extrasolar planets. Traub (2003) discusses the benefits of using color to broadly characterize the types of planets detected by Terrestrial Planet Finder and other similar missions. Similar to his analysis, we used data from Irvine et al. (1968) and Karkoschka (1994) to reproduce the colors of terrestrial and Jovian worlds. We additionally presented photometric observations of the Earth, Moon, and Mars taken with the DI spacecraft. Our data improves upon Traub's study, in which Earth's colors were from Earthshine and modeled Earth spectra and Mars' colors from ground based data that is contaminated by the terrestrial atmosphere.

Traub proposed using a color-color diagram and defined three broadband filters: 400 to 600, 600 to 800, and 800 to 1000 nm. Although his choice of bandpasses separates planets into groups, he acknowledges that the filter selection could be improved upon. The DI HRI afforded us the opportunities to observe Earth, Moon, and Mars from space, explore a range of filter combinations, and to determine the optimal filters for distinguishing between different types of planets. We chose the three filter combinations that reveal Earth's unique characteristics and partitioned the solar system bodies into color groups. Figure 9 shows the resulting color-color diagram of the reflectance of eight planets plus Titan and the Moon through the HRI 350, 550, and 850 nm filters. The ratio between the 350 and 550 nm filters is plotted on the vertical-axis and the ratio between the 850 and 550 nm filters is plotted on the horizontal axis. The lines where these ratios are equal to unity are also shown and the Sun's position is at their intersection.

### Figure 9

The ratio between the 350 and 550 nm filter in Figure 9 characterizes blue and UV reflectance. Earth, Uranus, and Neptune fall above or near the line of unity, meaning that they are blue or white. The increase towards UV wavelengths in the reflectance of these worlds is due to Rayleigh scattering in their atmospheres. Uranus and Neptune also have Raman scattering and H<sub>2</sub>S or hydrocarbon absorption in their atmospheres consequently reducing the effect of Rayleigh scattering. If H<sub>2</sub>S and other hydrocarbons were not present in the atmospheres of Uranus and Neptune, the planets would have 30-40% higher reflectance at shorter wavelengths. Earth is therefore the bluest of the planets because it has no absorbing species that counter Rayleigh scattering. This suggests that the ratio of reflectance at 350 and 550 nm could be used to detect the presence of a Rayleigh scattering atmosphere. However, the ratio is limited in determining the absence of Rayleigh scattering. As seen in the spectrum of Saturn, atmospheric absorption can overpower the effects Rayleigh scattering and result in a decrease in UV reflectance.

some of the same physical processes responsible for Earth's colors are present on the extrasolar world. Future work will explore the effects of different combinations of physical processes on the colors of extrasolar planets. Model spectra of various potential planets may help determine if our filter choices are optimal for extrasolar planet characterization.

## 6. Conclusion

This work uses EPOCH HRI observations of the Earth, Moon, and Mars in addition to previous full-disk observations of the other six solar system planets and Titan to analyze the limitations of using photometric colors to characterize extrasolar planets. We determined that the 350, 550, and 850 nm HRI filters were optimal for characterizing planetary colors by producing a color-color plot using relative full-disk reflectance through these filters. The ratio between the 350 and 550 nm filters can be used to determine the presence of Rayleigh scattering with all the bodies containing appreciable Rayleigh scattering having  $350:550 > 1$ . The ratio between 850 and 550 nm filters divides the worlds into three groups: those with strong methane absorbing atmospheres, with non-absorbing cloudy atmospheres, and with no atmospheres. The effect of using all three filters is that Earth is unique because it is the only body with a Rayleigh scattering non-absorbing cloudy atmosphere in our solar system as gleaned from disk-integrated observations.

Using these photometric colors, we find the Earth is easily distinguished from other solar system planets. As in this study, detailed conclusions that can be drawn about exoplanet atmospheres simply from a color-color plot are limited due to potentially competing physical processes in the atmosphere. For example, there are multiple mechanisms that can produce low UV reflectance and high IR reflectance. In the UV, both aerosol absorption and charge transfer with surface materials cause a decrease in relative reflectance. In the IR, both cloudy, non-absorbing atmospheres and crystal field absorptions on planetary surfaces produce 850:550 ratios greater than one. We are able to distinguish between the different physical processes responsible for planetary colors only through analysis of higher resolution spectroscopy. Nevertheless, a generation of telescopes capable of collecting such photometric observations can serve a critical role in first order characterization and constraining the population of Earth-like extrasolar planets. Such missions will function as a cost efficient precursor for guiding the next generation of missions with advanced spectroscopic capabilities.

## References

- A'Hearn, Michael. 2008, in 37<sup>th</sup> COSPAR Scientific Assembly, 2
- Arnold, L., Gillet, S., Lardièrre, Riaud, P., & Schneider, J. 2002, *A&A*, 392, 231-237
- Arnold, L. 2008, *Space Science Review*, 135, 323-333

- Grinspoon, D. H., Williams, D. M., Piccioni, G., Bertaux, J., & Moore, C. 2008, *BAAS* 40, 386
- Hampton, D., Baer, J. W., Huisjen, M. A., Varner, C. C., Delamere, A., Wellnitz, D. D., A'Hearn, M. F., & Klaasen, K. P. 2005, *Space Science Reviews*, 117, 43-93
- Hillier, J. K., Buratti, B. J., & Hill, K. 1999, *Icarus*, 141, 205-225
- Irvine, W. M., Simon, T., Menzel, D. H., Charon, J., Leconte, G., Griboval, P., & Young, A. T. (1968a), *AJ*, 73, 251-264
- Irvine, W. M., Simon, T., Menzel, D., Pikoos, C., & Young, A. 1968b, *AJ*, 73, 807-828
- Josset, J.-L. 2008, in 37th COSPAR Scientific Assembly, 1414
- Karkoschka, E. 1994, *Icarus*, 111, 174-192
- Karkoschka, E. 1998, *Icarus*, 133, 134-146
- Klaasen, K. P., A'Hearn, M. F., Baca, M., Delamere, A., Desnoye, M., Farnham, T., Groussin, O., Hampton, D., Ipatov, S., Li, J.-Y., Lisse, C., Mastrodemos, N., McLaughlin, S., Sunshine, J., Thomas, P., & Wellnitz, D. 2008, *Review of scientific instruments*, 79, 77
- Knollenberg, R., Travis, L., Tomasko, M., Smith, P., Ragent, B., Esposito, L., McCleese, D., Martonchik, J., & Beer, R. 1980, *Journal of Geophysical Research*, 85, 8059-8081
- Levine, M., Lisman, D., Shaklan, S., Kasting, J., Traub, W., Alexander, J., Angel, R., Blaurock, C., Brown, M., Brown, R., Burrows, C., Clampin, M., Cohen, E., Content, D., Dewell, L., Dumont, P., Egerman, R., Ferguson, H., Ford, V., Greene, J., Guyon, O., Hammel, H., Heap, S., Ho, T., Horner, S., Hunyadi, S., Irish, S., Jackson, C., Kasdin, J., Kissil, A., Krim, M., Kuchner, M., Kwack, E., Lillie, C., Lin, D., Liu, A., Marchen, L., Marley, M., Meadows, V., Mosier, G., Mouroulis, P., Noecker, M., Ohl, R., Oppenheimer, B., Pitman, J., Ridgway, S., Sabatke, E., Seager, S., Shao, M., Smith, A., Soummer, R., Stapelfeldt, K., Tenerell, D., Trauger, J., & Vanderbei, R. 2009, *Terrestrial Planet Finder Coronagraph (TPF-C) Flight Baseline Concept*, arXiv:0911.3200
- Livengood, T., A'Hearn, M., Deming, D., Charbonneau, D., Barry, R., Hewagama, T., Lisse, C., McFadden, L., Meadows, V., Seager, S., Wellnitz, D., & EPOXI-EPOCh Science Team. 2009, in *AAS DPS Meeting* 41
- Lucey, P. G., Taylor, G. J., & Hawke, B. R. 1998, *J. Geophys. Res.*, 103, 3701-3708
- Marov, M. Ya., Avduevsky, V. S., Borodin, N. F., Ekonomov, A. P., Kerzhanovich, V. V., Lysov, V. P., Moshkin, B. Ve., Rozhdestvensky, M. K., & Ryabov, O. L. 1973, *Icarus*, 20 407-421
- Marov, M. Ya. 1978, *Annual Review Astronomy and Astrophysics*, 16, 141-169
- Maxwell, T. & Andre, C. 1981, in *Lunar and Planetary Science Conference Proceedings*, 12, 715-725

Tera, F., Papanastassiou, D., & Wasservurg, G. 1974, *Earth and Planetary Science Letters*, 22, 1-21

Traub, W. 2003, in *Conf. Towards Other Earths: Darwin/TPF and the Search for Extrasolar Planets*, ed. M. Fridlund & T. Henning (Heidelberg, Germany: ESA SP539) 231-240.

Trauger, J.T. & Traub, W. A. 2007, *Nature*, 446, 771-773

Tomasko, M. G., Doose, L. Engel, S., Dafoe, L. E., West, R., Lemmon, M., Karkoschka, E., & See, C. 2008, *Planetary and Space Science*, 56, 669-707

Vilas, F. 1985, *Icarus*, 64, 133-138

Weidenschilling, S. J., & Lewis, J. S. 1973, *Icarus*, 20, 465-476

West, R. A. 2007, in *Encyclopedia of the Solar System*, ed. L.A. McFadden, P. R. Weissman, & T.V. Johnson (2nd ed.; V. Amsterdam: Academic Press), 383 – 402

Youngkin, R. L. 1966, *ApJ*, 144, 809 - 818

NIR due to charge transfer of low-iron silicates. This figure demonstrates that Earth is the only body with an increase in reflectivity towards UV wavelengths due to Rayleigh scattering.

**Figure 7:** Karkoschka (1994) high-resolution spectrum of Jupiter overlaid with HRI-VIS filter transmission curves (Hampton et al. 2005).

**Figure 8:** Karkoschka (1994) high-resolution spectra and equivalent HRI reflectance values computed by convolution with HRI-VIS filter transmission functions. The reflectance of Jupiter, Saturn, and Titan have absorption due to aerosols in the UV. Uranus and Neptune have competing aerosol absorption and Rayleigh scattering causing their reflectivity to be flat UV spectra. All five bodies exhibit varying amounts of methane absorption in the NIR.

**Figure 9:** Color-color plot with ratio of reflectance in HRI 350 and 550 nm filters on the vertical axis and 850 and 550 nm filters on the horizontal axis. The lines of unity are plotted for reference and the Sun's radiance resides at the intersection of the two lines. Bodies with 350:550 >1 have atmospheres dominated by Rayleigh scattering and those with 350:550 <1 are dominated by atmospheric or charge-transfer absorption. Although 350:550 is diagnostic of the presence of Rayleigh scattering it is not sufficient to determine its absence. The 850:550 groups the bodies into three regions: (1) airless bodies on the right, (2) intermediate cloudy atmospheres near unity, and (3) strong NIR absorbing atmospheres on the left. The Earth is the only body that resides in the upper right quadrant of the diagram due to Rayleigh scattering in its intermediate cloudy atmosphere.

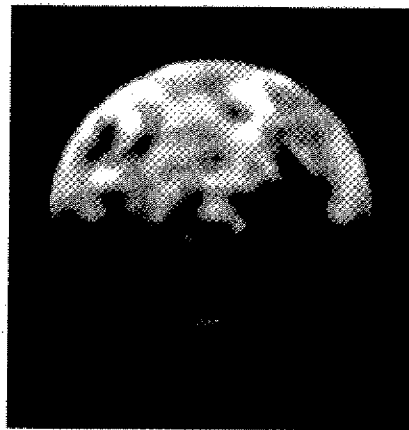


Fig. 1a Crow et al. 2010



Fig. 1 b      Fig. 1c  
intentionally  
not printed  
Crow et al 2010

# Lunar Regions Spectral Comparison

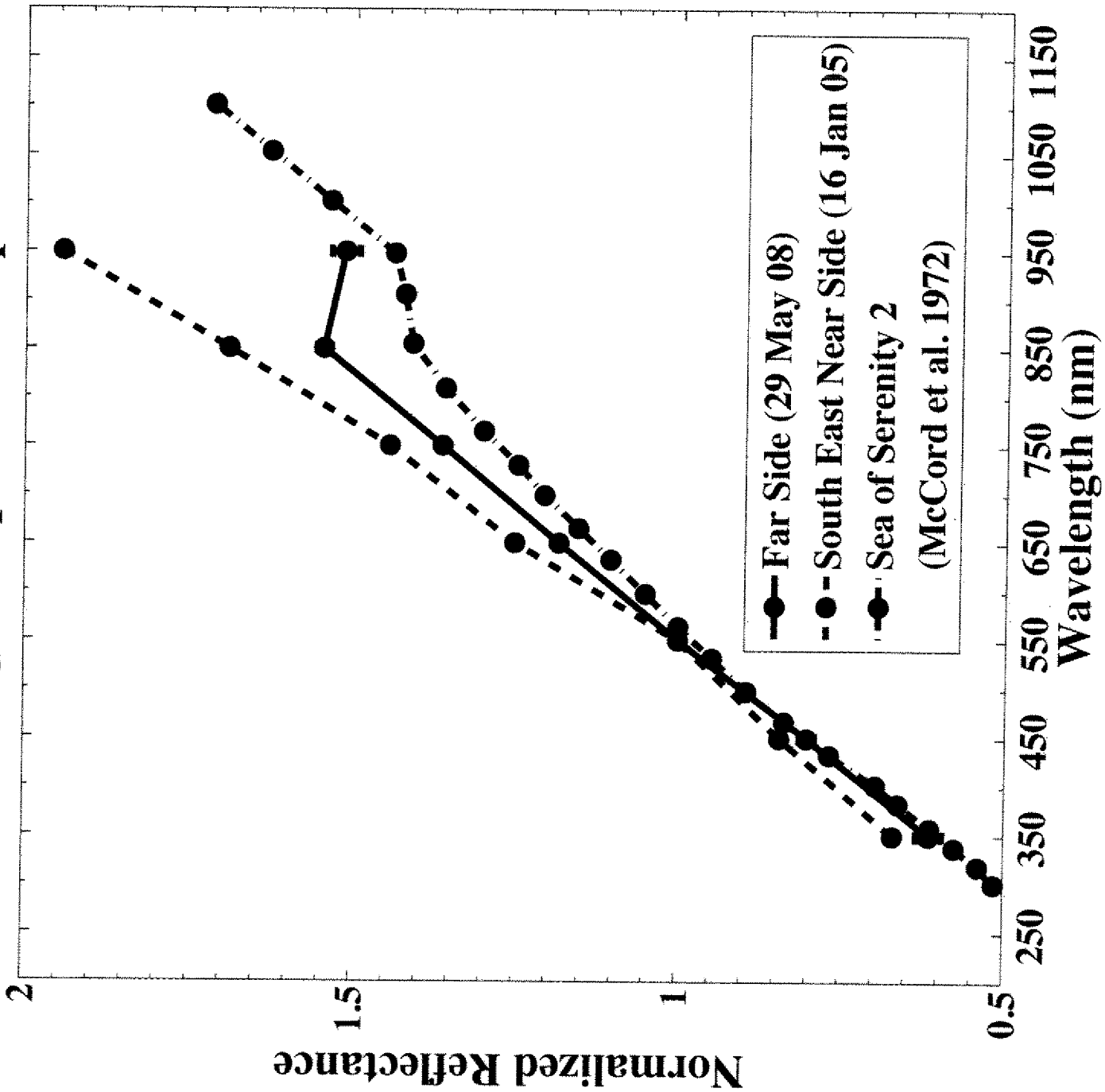


Fig. 2 Crew et al 2010

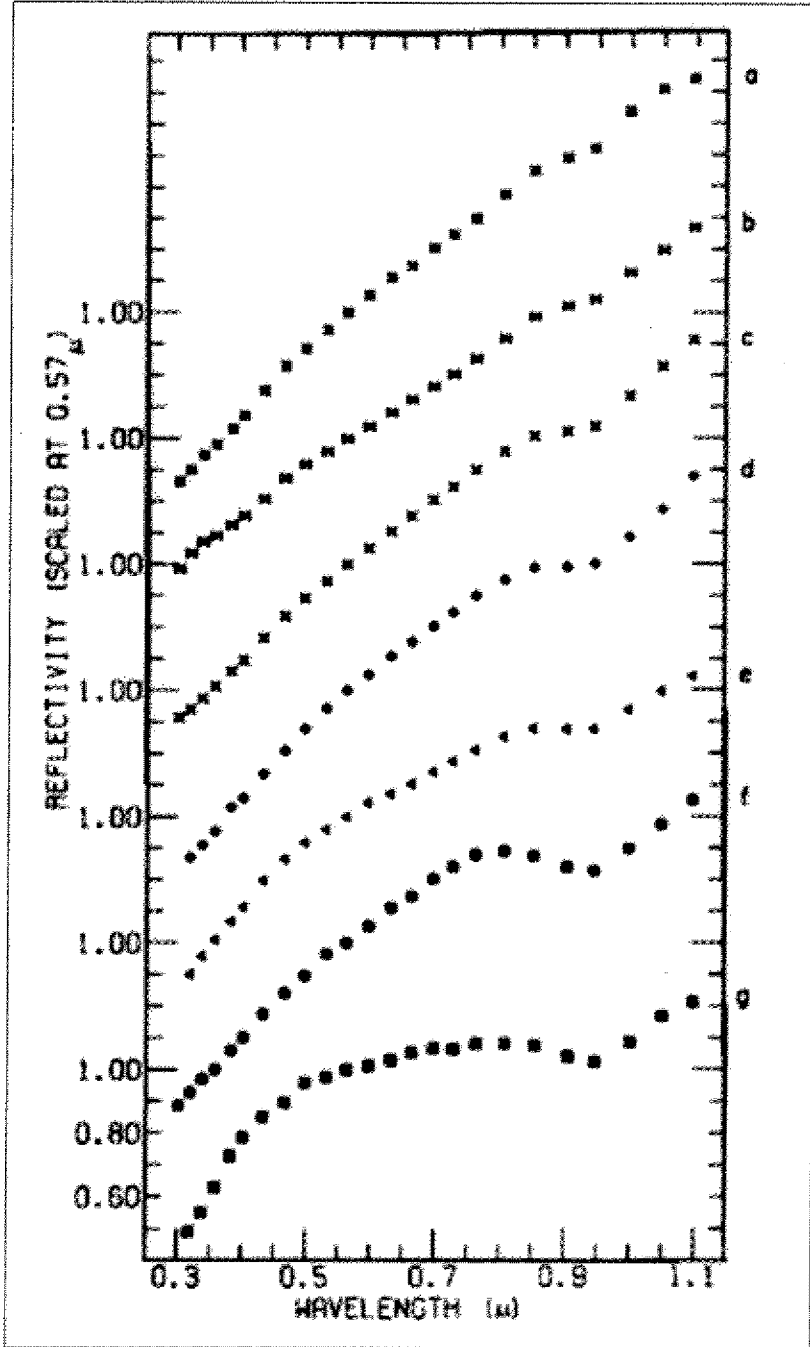


Fig. 3 Crow et al. 2010

# Reflectance of EPOCH Targets

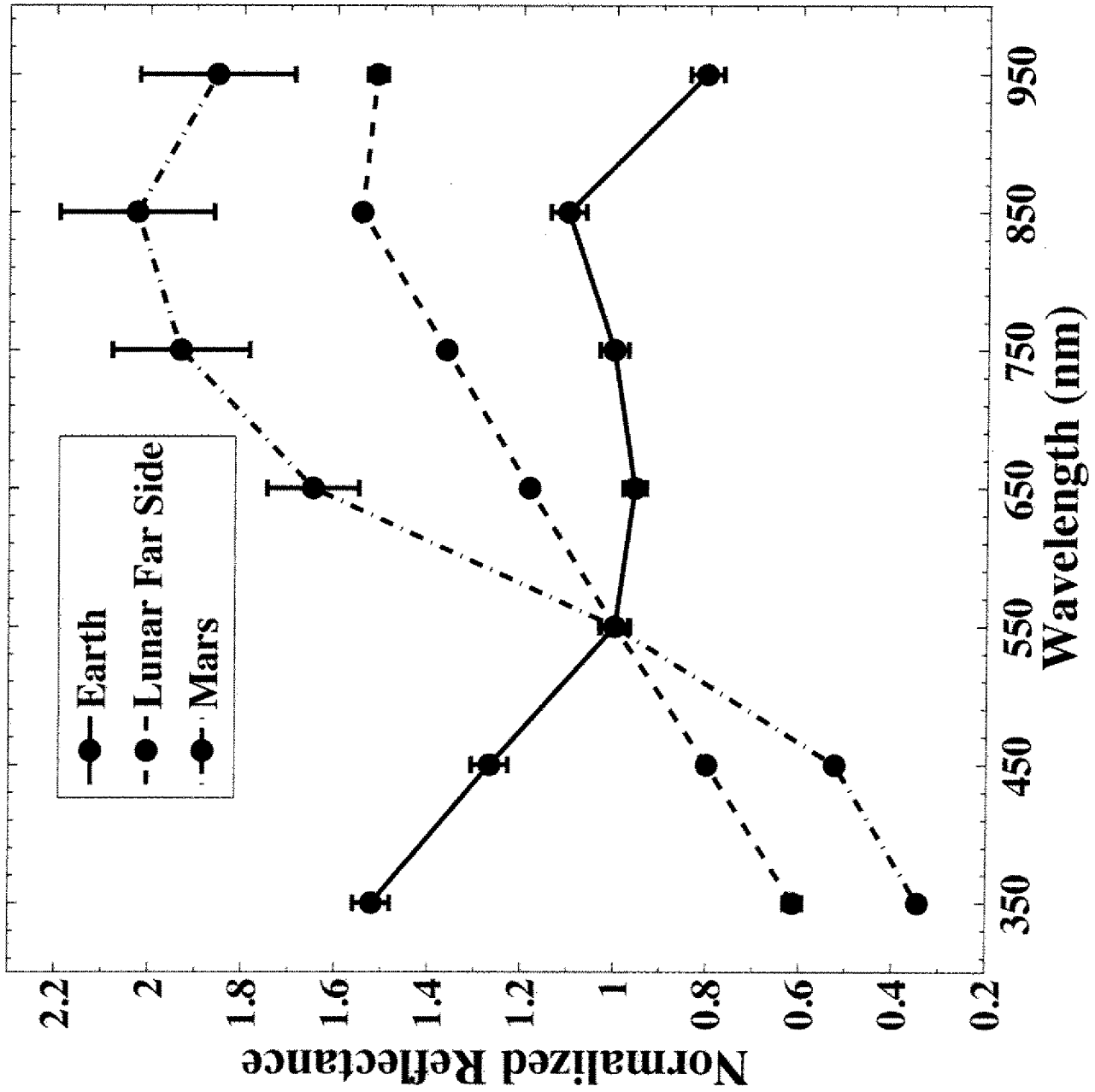


Fig. 4 Crow et al. 2010

# Rayleigh Scattering Model Comparison

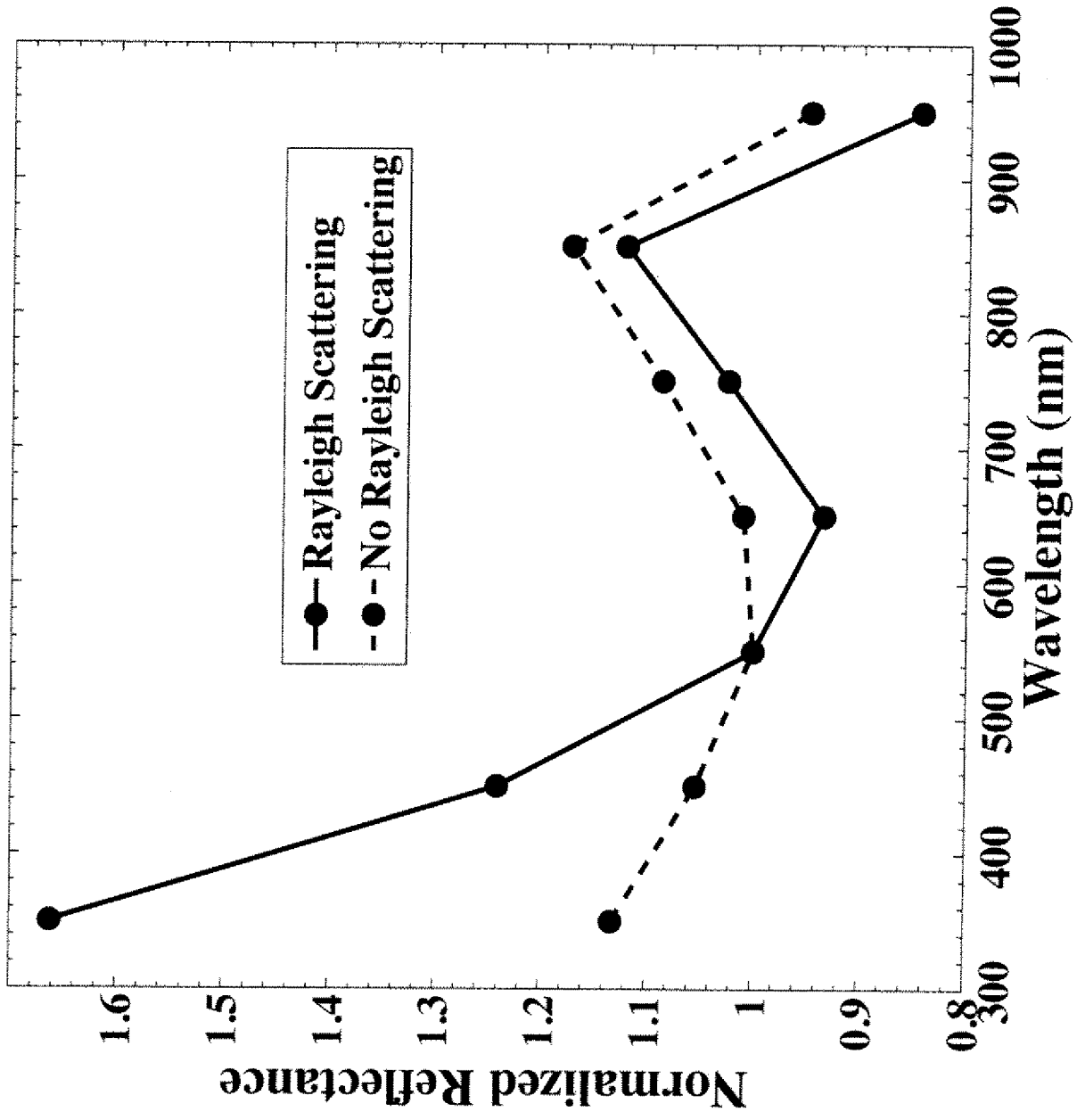


Fig 5 Crow et al. 2010

# Terrestrial Planets Spectral Comparison

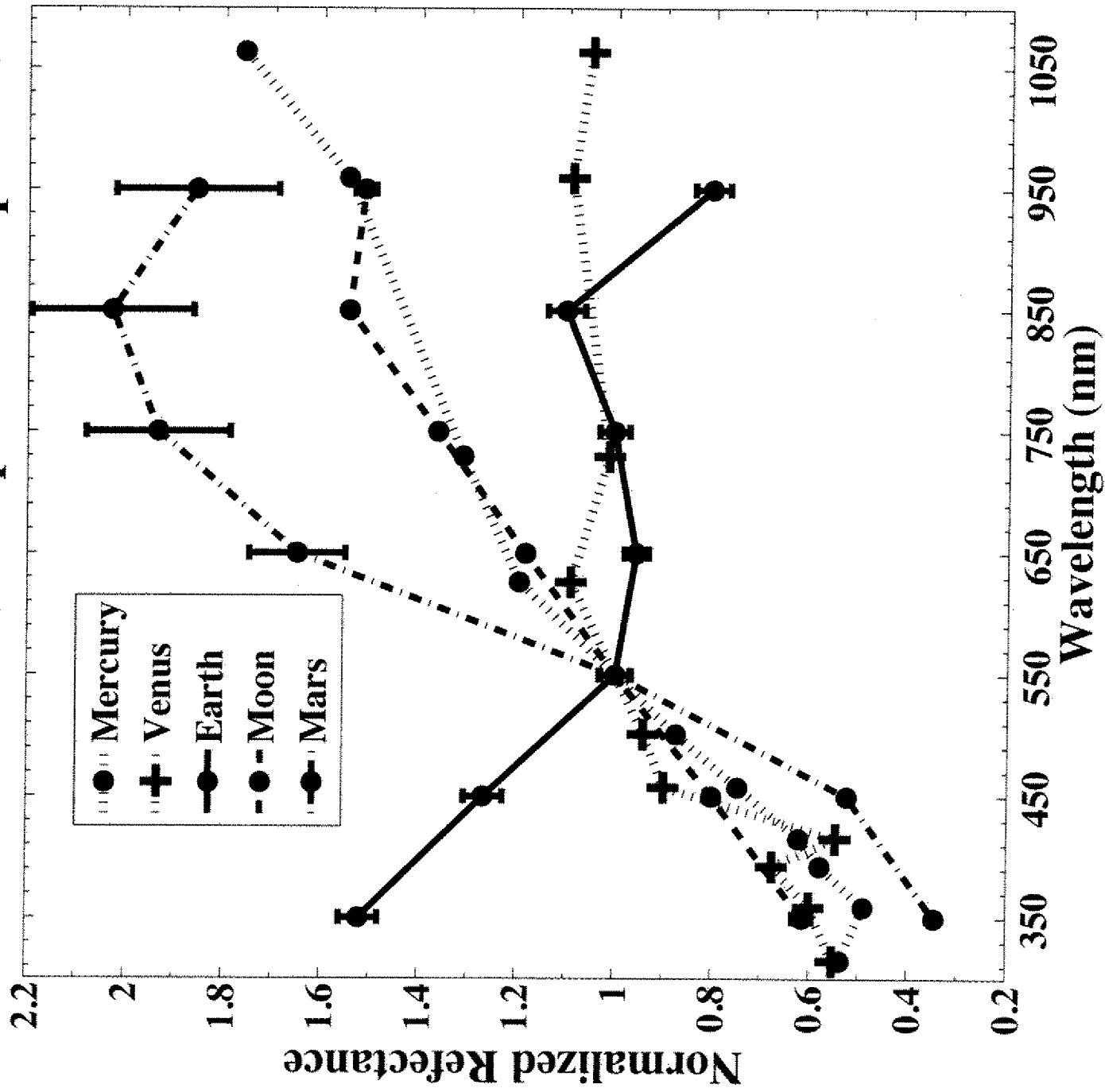


Fig. 6 Crow et al 2010

# Jupiter Data & HRI Filter Transmission

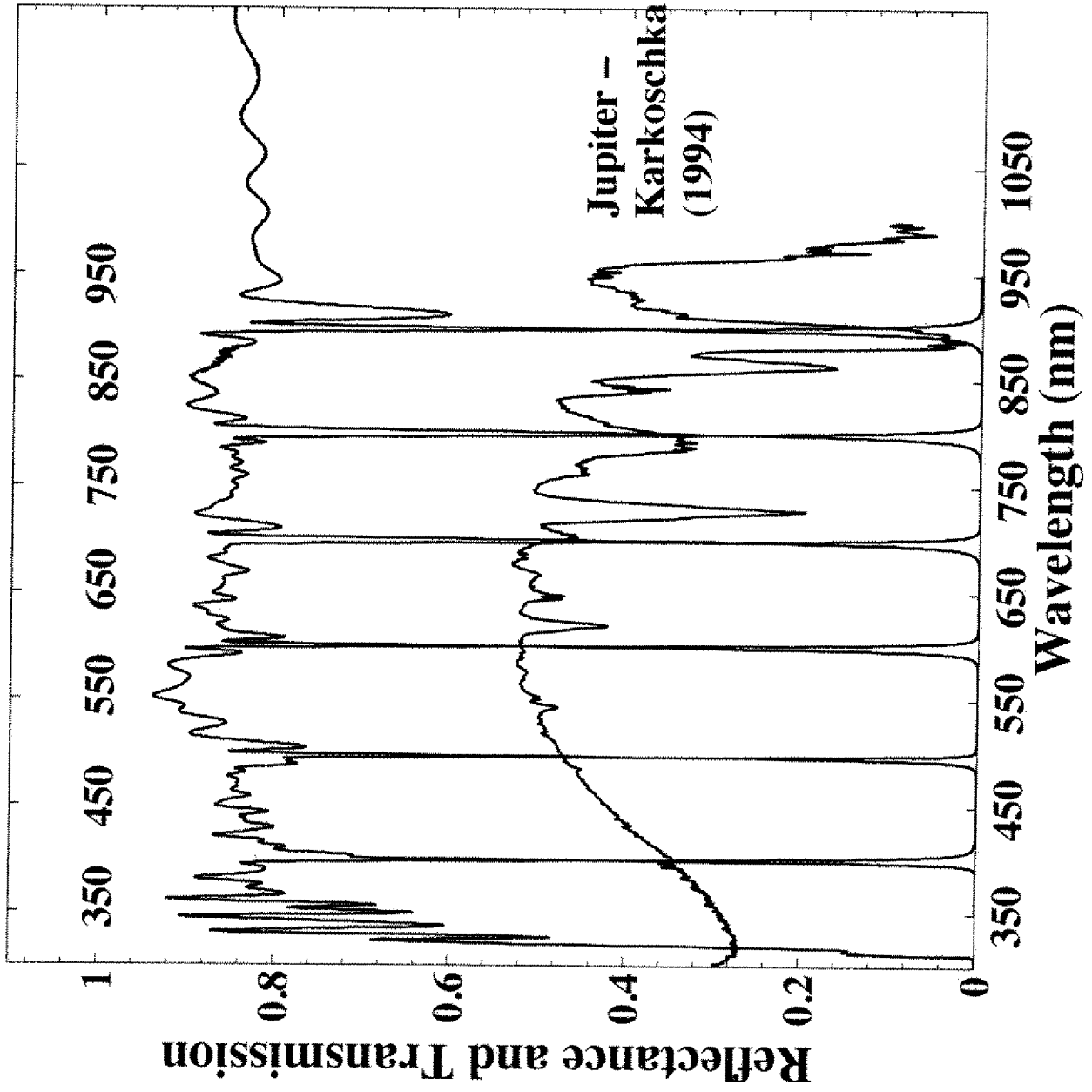


Fig. 7 Crow et al 2010

# HRI Convolved Karkoschka Spectra

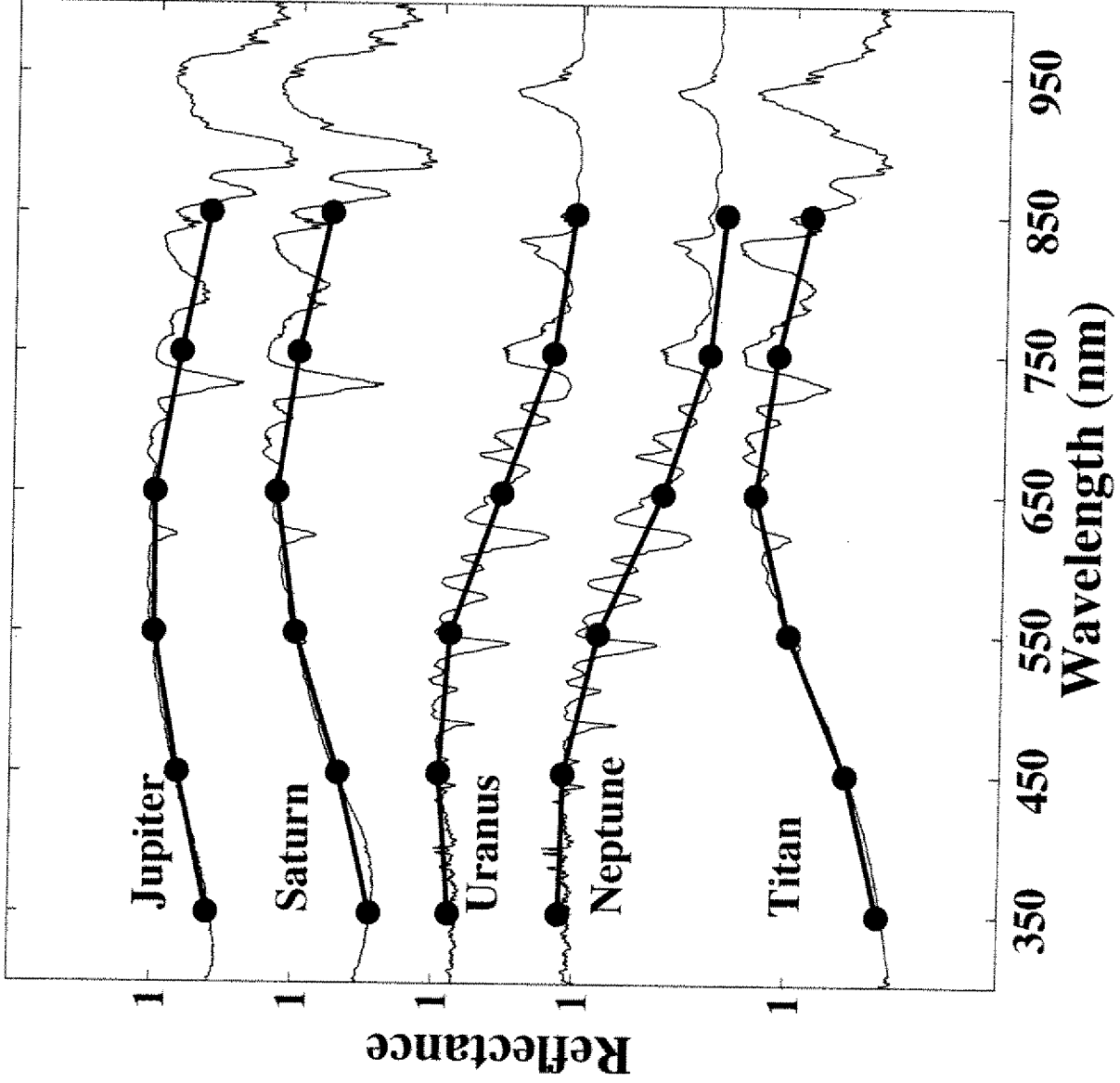


Fig. 8 Crowe et al 2010

# Color - Color Plot of Solar System Worlds

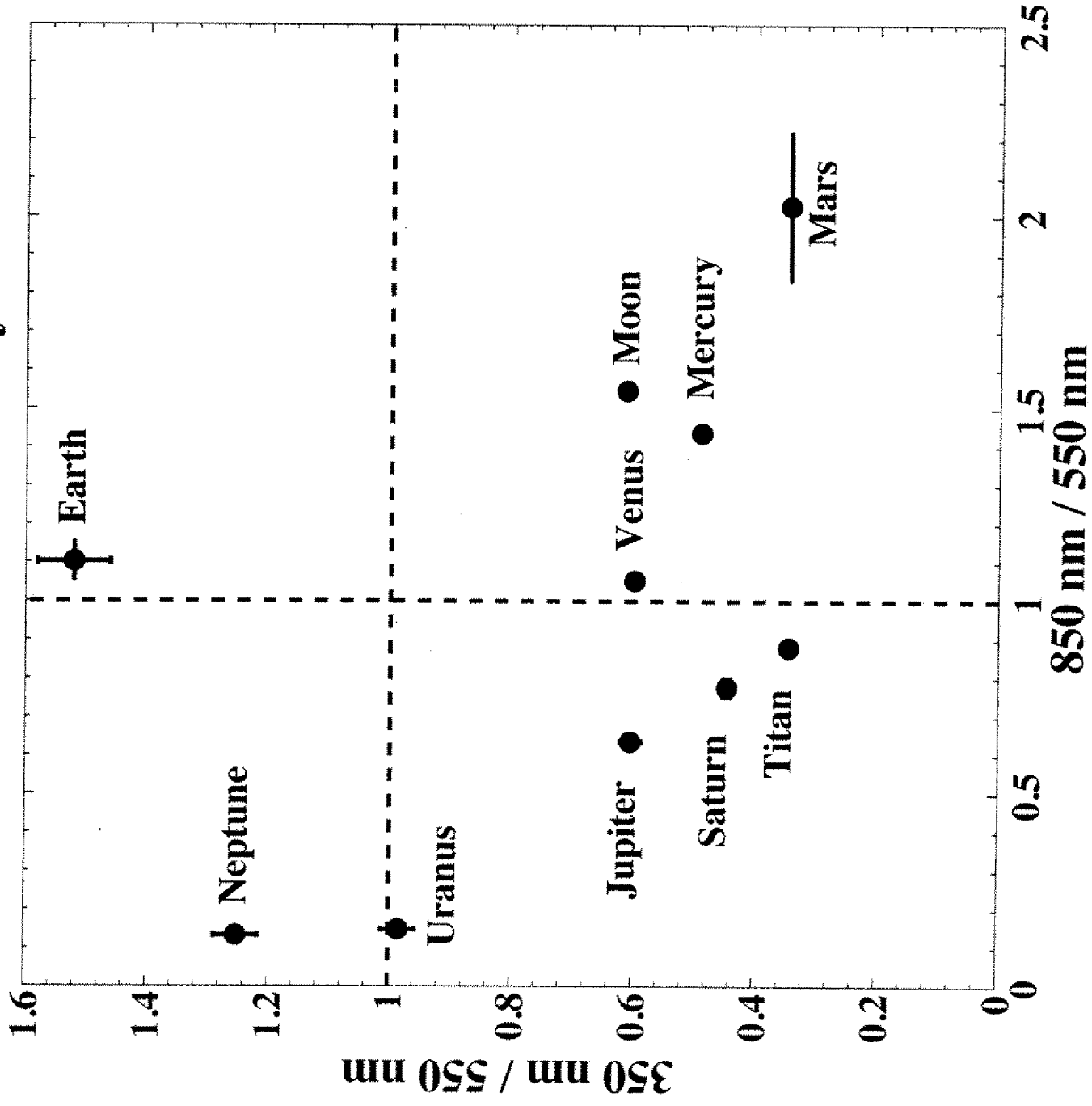
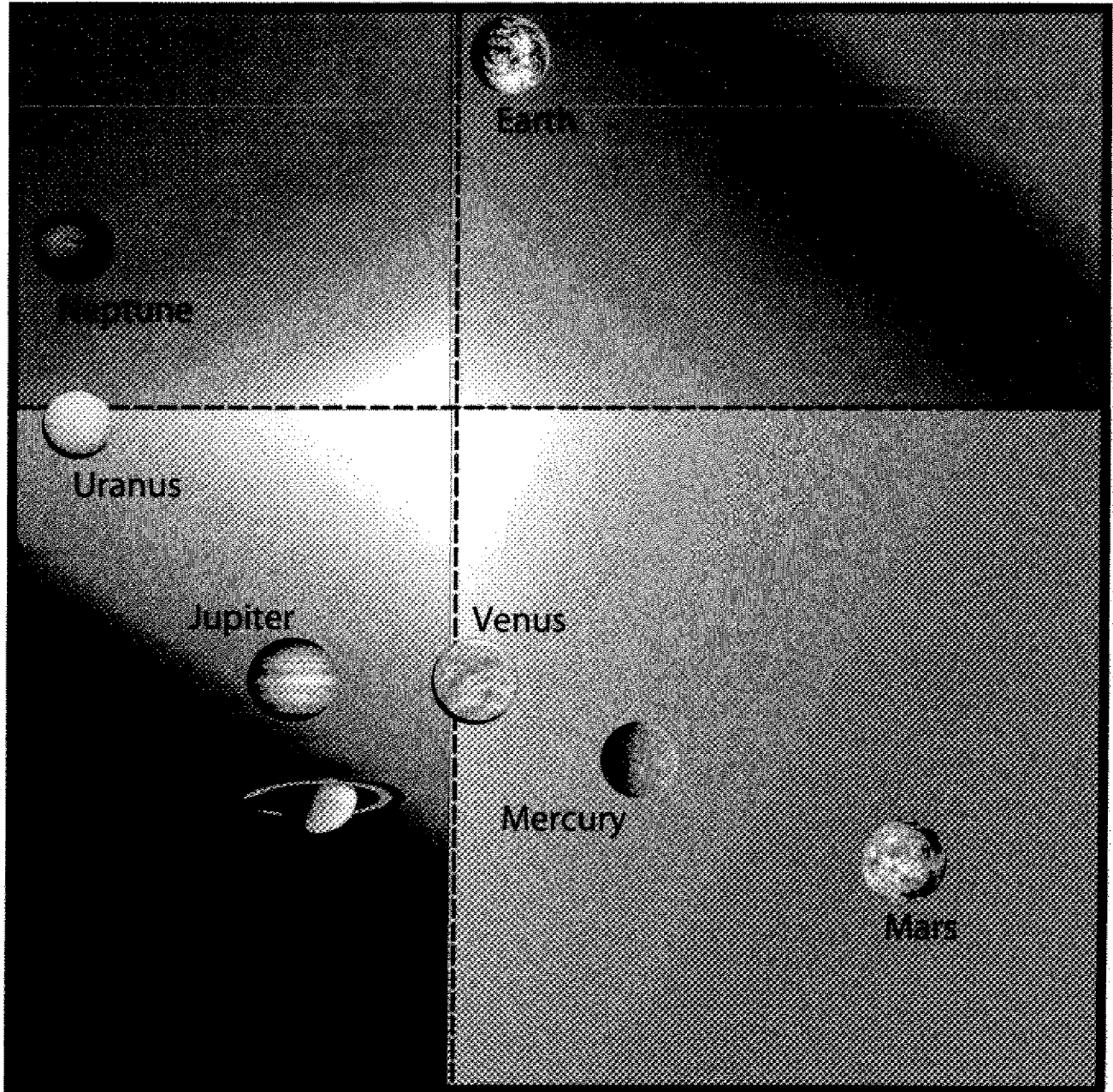


Fig 9 Crow et al 2010



draft  
Fig 9 for public presentation

Crow et al 2010